

SSL: A Self-similarity Loss for Improving Generative Image Super-resolution

Du Chen*

Department of Computing,
The Hong Kong Polytechnic University,
Hong Kong, China
OPPO Research Institute,
Shenzhen, China
csdud.chen@connect.polyu.hk

Jie Liang

OPPO Research Institute,
Shenzhen, China
liangjie3@oppo.com

Zhengqiang Zhang*

Department of Computing,
The Hong Kong Polytechnic University,
Hong Kong, China
OPPO Research Institute,
Shenzhen, China
zhengqiang.zhang@connect.polyu.hk

Lei Zhang[†]

Department of Computing,
The Hong Kong Polytechnic University,
Hong Kong, China
OPPO Research Institute,
Shenzhen, China
cslzhang@comp.polyu.edu.hk

Abstract

Generative adversarial networks (GAN) and generative diffusion models (DM) have been widely used in real-world image super-resolution (Real-ISR) to enhance the image perceptual quality. However, these generative models are prone to generating visual artifacts and false image structures, resulting in unnatural Real-ISR results. Based on the fact that natural images exhibit high self-similarities, i.e., a local patch can have many similar patches to it in the whole image, in this work we propose a simple yet effective self-similarity loss (SSL) to improve the performance of generative Real-ISR models, enhancing the hallucination of structural and textural details while reducing the unpleasant visual artifacts. Specifically, we compute a self-similarity graph (SSG) of the ground-truth image, and enforce the SSG of Real-ISR output to be close to it. To reduce the training cost and focus on edge areas, we generate an edge mask from the ground-truth image, and compute the SSG only on the masked pixels. The proposed SSL serves as a general plug-and-play penalty, which could be easily applied to the off-the-shelf Real-ISR models. Our experiments demonstrate that, by coupling with SSL, the performance of many state-of-the-art Real-ISR models, including those GAN and DM based ones, can be largely improved, reproducing more perceptually realistic

image details and eliminating many false reconstructions and visual artifacts. Codes and supplementary material are available at <https://github.com/ChrisDud0257/SSL>.

CCS Concepts

• Computing methodologies → Reconstruction.

Keywords

image super-resolution, generative adversarial networks, generative diffusion models, self-similarity loss

ACM Reference Format:

Du Chen, Zhengqiang Zhang, Jie Liang, and Lei Zhang. 2024. SSL: A Self-similarity Loss for Improving Generative Image Super-resolution. In *Proceedings of the 32nd ACM International Conference on Multimedia (MM '24)*, October 28–November 1, 2024, Melbourne, VIC, Australia. ACM, New York, NY, USA, 10 pages. <https://doi.org/10.1145/3664647.3680874>

1 Introduction

Image super-resolution (ISR) is a fundamental problem in low-level vision. Given a low-resolution (LR) input, ISR aims to recover its high-resolution (HR) counterpart with high fidelity in contents, which has a wide range of applications in digital photography [28], high definition display [83], medical image analysis [27], remote sensing [34], etc. Starting from SRCNN [13], various convolutional neural network (CNN) based methods have been proposed to improve the ISR performance, such as residual connections [22, 31, 39, 42], dense connections [91] and channel-attention [23, 90]. Recently, some transformer-based ISR methods [7–9, 17, 40, 89] have also emerged and demonstrated more powerful performance.

In the early stage, researchers usually employed simple degradations, such as bicubic downsampling and downsampling after Gaussian smoothing, to synthesize the LR-HR training pairs, while focusing on the study of ISR network design. However, the image degradations in real-world are much more complex, and the ISR

*Both authors contributed equally to the paper

[†]Corresponding author

Permission to make digital or hard copies of all or part of this work for personal or classroom use is granted without fee provided that copies are not made or distributed for profit or commercial advantage and that copies bear this notice and the full citation on the first page. Copyrights for components of this work owned by others than the author(s) must be honored. Abstracting with credit is permitted. To copy otherwise, or republish, to post on servers or to redistribute to lists, requires prior specific permission and/or a fee. Request permissions from permissions@acm.org.
MM '24, October 28–November 1, 2024, Melbourne, VIC, Australia.

© 2024 Copyright held by the owner/author(s). Publication rights licensed to ACM.
ACM ISBN 979-8-4007-0686-8/24/10
<https://doi.org/10.1145/3664647.3680874>

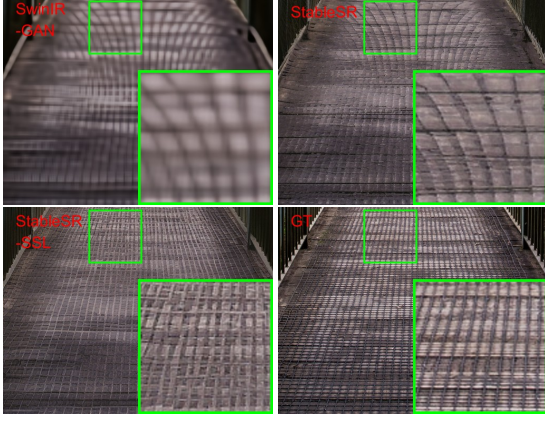


Figure 1: From left to right and top to bottom: the Real-ISR results generated by SwinIRGAN [40], StableSR [63], our SSL guided StableSR and the ground-truth (GT) image. SwinIRGAN produces over-smoothed and wrong results, while StableSR produces more details but with false structures and artifacts. Our SSL guided StableSR generates more faithful details while suppressing much the artifacts.

models trained on those simple synthetic data can hardly be generalized to real-world applications. Therefore, in recent years many works have been done on real-world ISR (Real-ISR), aiming to obtain perceptually realistic ISR results on degraded images in real-world scenarios [10, 19, 36–38, 45, 53, 64, 65, 71, 73, 77, 80, 82, 85, 93]. Some researchers proposed to collect real-world LR-HR image pairs by using long-short camera focal lengths [4, 5, 69, 70, 74, 75, 88]; however, this is very costly and the trained models may only work well when similar photographing devices are used. Therefore, researchers propose to synthesize more realistic training data by designing more complex degradation models. The notable works include BSRGAN [84] and Real-ESRGAN [65]. In BSRGAN [84], Zhang et al. randomly shuffled and combined blur, downsampling and noise degradations to form a complex degradation, while in Real-ESRGAN [65], Wang et al. developed a high-order degradation model with several repeated degradation operations. Recently, researchers have also proposed to introduce human guidance into the training data generation process [6].

Given the training data with more realistic degradations, another issue is how to train the network to achieve the goal of Real-ISR. It is well-known that the L_1 or L_2 loss, which aims to minimize the fidelity error, often results in over-smoothed image details. To tackle this issue, in the past a few years, the generative adversarial networks (GANs) [18] have been widely adopted to train Real-ISR models [33, 35, 41, 46, 52, 66, 67, 87]. With the help of adversarial loss, GAN models can learn to find an image reconstruction path to generate more sharp details. Though great progress has been made, one critical limitation of GAN based Real-ISR models remain, *i.e.*, they incline to hallucinate visually unpleasant artifacts. Very recently, with the rapid development of diffusion models (DMs) [25, 59], it becomes popular to leverage the pre-trained large scale text-to-image models, such as stable diffusion (SD) [55], to achieve Real-ISR. Benefiting from the strong generative priors in DMs, some

recent works [56, 63, 79] have demonstrated encouraging Real-ISR results with fine-scale and realistic details. However, DMs have high randomness, which lead to unstable Real-ISR outputs and false image details.

In this paper, we aim to improve the GAN and DM based Real-ISR methods, reducing the artifacts and producing more realistic details, by proposing a new training loss function. It is well-known that natural images exhibit repetitive patterns across the whole image. Such a property of self-similarity has been extensively used in many image restoration algorithms, such as BM3D [11], NCSR [15], WNNM [21], and NLSN [49], where the image self-similarity is used as a prior to regularize the restored image. In this work, we employ the image self-similarity property as a powerful penalty to supervise the Real-ISR training progress. The proposed image self-similarity loss (SSL) could act as a plug-and-play penalty in most of the existing generative Real-ISR models, guiding them to exploit more effectively the inherent image self-similarity information for detail reconstruction. Specifically, we compute a self-similarity graph (SSG) to describe the image structural dependency, and minimize the distance between the SSGs of the ground-truth (GT) and Real-ISR output to optimize the model. To make the training process more efficient and focus more image edge/texture areas, we generate an edge mask from the GT image in an offline manner, and only build the SSG upon the edge pixels.

Our proposed SSL can be easily adopted into the off-the-shelf GAN-based and DM-based Real-ISR models as an extra penalty to enhance image details and reduce the unpleasant artifacts. An example is shown in Fig. 1. One can see that SwinIRGAN [40] over-smooths the image textures and generates wrong details, while the recent DM-based StableSR [63] restores much clearer details but still fails to generate some fine scale structures or correct textures. In comparison, the StableSR model trained with our SSL could reconstruct both clear content and more realistic textures with better perception quality. Our extensive experiments on state-of-the-art Real-ISR models validate the effectiveness of our proposed SSL, either in GAN-based or DM-based ISR tasks.

2 Related Work

Traditional Fidelity-Oriented ISR. Since SRCNN [13], many CNN backbones have been developed to promote the ISR performance in terms of PSNR and SSIM [68] measures. EDSR [42] and RDN [91] incorporate residual and densely connections, respectively. RCAN [90], OA-DNN [16], CRAN [92] and HAN [51] make use of channel/spatial attention modules. Recently, transformer-based models have shown stronger ability towards long-range dependency modeling. SwinIR [40] utilizes shifted partition windows to compute the image self-attention. ELAN [89] introduces multi-scale self-attention blocks to extract long-distance dependency. ACT [78] utilizes CNN to extract local interaction and transformer to obtain long-range dependency.

GAN-based Generative Real-ISR. The fidelity-oriented ISR models often generate over-smoothed details, sacrificing the perceptual quality of natural images. Inspired by GAN[18], many generative ISR methods have been proposed to obtain more photo-realistic results. SRGAN [33], and ESRGAN [67] utilize VGG-style [58] discriminator to perform the adversarial training. BSRGAN [84] and

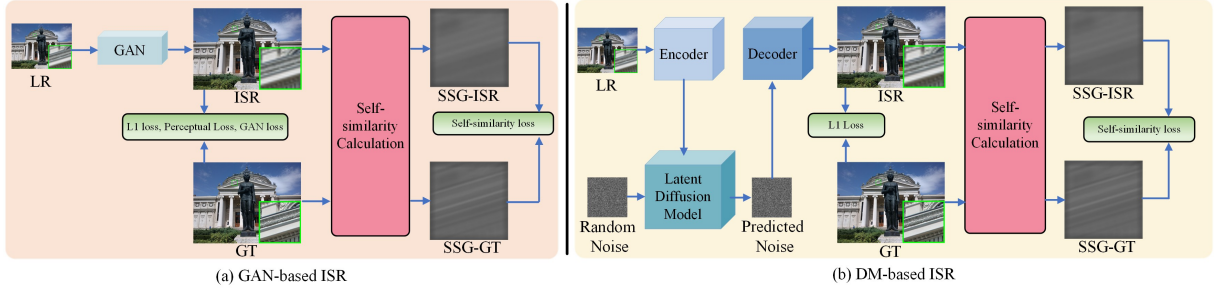


Figure 2: Illustration of the training progress of (a) generative adversarial network (GAN) based and (b) latent diffusion model (DM) based Real-ISR by using our proposed self-similarity loss (SSL). The GAN or DM network is employed to map the input LR image to an ISR output. We calculate the self-similarity graphs (SSG) of both ISR output and ground-truth (GT) image, and calculate the SSL between them to supervise the generation of image details and structures.

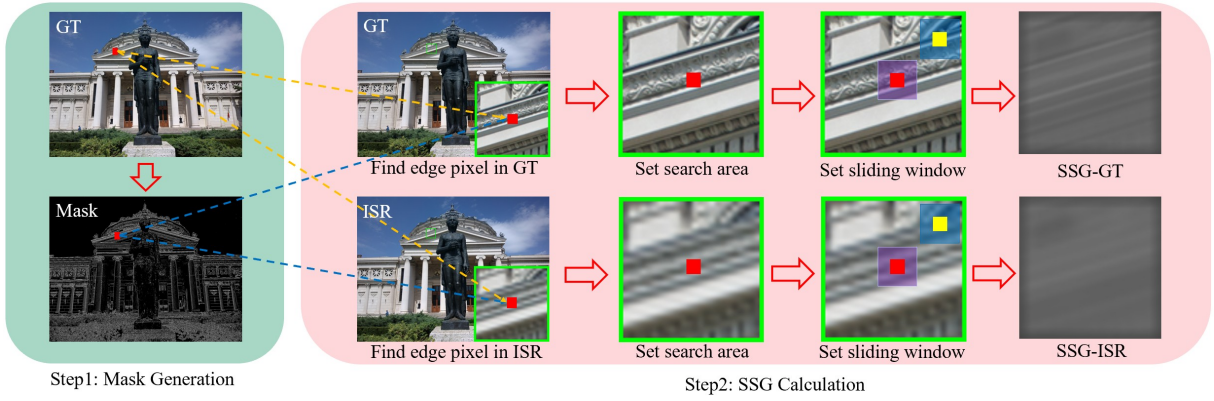


Figure 3: Illustration of the self-similarity graph (SSG) computing process. We first generate a mask to indicate the image edge areas by applying the Laplacian Operator on the GT image. During the training period, for each edge pixel in the mask, we find the corresponding pixels in the GT image and ISR image, and set a search area centred at them. A local sliding window is utilized to calculate the similarity between each pixel in the search area and the central pixel so that an SSG can be respectively computed for the GT image and the ISR image, with which the SSL can be computed. The red pixel means the edge pixel, while the blue block means the sliding window.

Real-ESRGAN [65] introduce complex degradation processes to synthesize the real-world degradation. HGGT [6] annotates positive and negative training pairs to enhance the perceptual quality in GAN training progress. In order to make the GAN training process more stable, SROBB [54] presents an enhanced perceptual loss to restrain the model with different semantic labels. SPSR [46] embeds the well-extracted structure prior into the RRDB network [67]. RankSRGAN [87] firstly trains a ranker model to indicate the relative perception quality of an image, and then utilizes a well-trained ranker to guide the generator to reconstruct better details. BebyGAN [35] searches the best candidate GT patch in the neighborhood to perform LR-HR supervision. LDL [41] computes an artifact map to indicate the local artifacts in ISR outputs, then imposes appropriate penalty on the artifact areas to improve the perceptual quality.

DM-based Generative Real-ISR. The powerful generative priors embedded in DMs can be exploited for Real-ISR. SR3 [56] utilizes a conditional pixel-level DM to iteratively denoise and generate

super-resolved results. StableSR [62] performs Real-ISR in the latent diffusion space by using a controllable feature wrapping module to balance between the reconstruction fidelity and the perceptual quality. PASD [76] introduces a pixel-aware cross attention block as a controllable module to guide the high-quality details generation. DiffBIR [43] utilizes a two-stage model, which first reduces complicated degradation factors and then uses the well-trained generative prior in SD to reconstruct delicate contents. DiffIR [72] pre-trains a DM with high-quality GT images to obtain abundant priors and then finetunes the DM with their low-quality counterparts to complete the Real-ISR task. ResShift [79] adopts an efficient sampling strategy through shifting the residual between high-quality and low-quality images to largely accelerate the diffusion steps.

3 Image Self-similarity Loss

The proposed training framework is illustrated in Fig. 2. In addition to the commonly used L_1 , perceptual loss, adversarial loss in GAN-based methods, or the Gaussian noise prediction MSE loss in

Table 1: Quantitative results of seven representative GAN-based Real-ISR models and their counterparts coupled with the proposed SSL. The bicubic degradation model is used here. For each of the seven groups of comparisons, the better results are highlighted in boldface. The PSNR and SSIM indices are computed in the Y channel of Ycbr space.

Method		ESRGAN	ESRGAN -SSL	RankSR GAN	RankSR GAN-SSL	SPSR	SPSR -SSL	Beby GAN	Beby GAN-SSL	LDL	LDL -SSL	ELAN GAN	ELAN GAN-SSL	SwinIR GAN	SwinIR GAN-SSL
Training Dataset		DF2K_OST		DIV2K		DIV2K		DF2K		DF2K		DIV2K		DF2K	
Set5	PSNR↑	30.4378	30.7786	29.6518	30.1834	30.3967	30.4476	30.4951	31.0239	31.0332	31.1106	30.7134	30.7942	31.0982	31.1616
	SSIM↑	0.8523	0.8582	0.8379	0.8517	0.8443	0.8458	0.8550	0.8652	0.8611	0.8660	0.8526	0.8588	0.8686	0.8702
	LPIPS↓	0.0739	0.0621	0.0699	0.0675	0.0615	0.0598	0.0595	0.0583	0.0660	0.0617	0.0547	0.0528	0.0682	0.0594
	DISTS↓	0.0970	0.0929	0.1038	0.1014	0.0924	0.0906	0.0912	0.0906	0.0934	0.0924	0.0854	0.0840	0.0977	0.0936
Set14	PSNR↑	26.2786	26.7148	26.4514	26.6163	26.6423	26.6410	26.8625	27.1674	26.9378	27.1195	26.9128	27.0785	27.0486	27.3178
	SSIM↑	0.6992	0.7114	0.7030	0.7132	0.7138	0.7091	0.7270	0.7272	0.7212	0.7263	0.7242	0.7287	0.7314	0.7385
	LPIPS↓	0.1314	0.1202	0.1350	0.1337	0.1303	0.1331	0.1204	0.1200	0.1198	0.1169	0.1144	0.1123	0.1201	0.1114
	DISTS↓	0.0985	0.0937	0.1104	0.1065	0.0990	0.0960	0.0930	0.0937	0.0917	0.0924	0.0940	0.0934	0.0983	0.0962
DIV2K100	PSNR↑	28.1983	28.7341	28.0314	28.3523	28.2042	28.5881	28.6301	29.1332	28.8401	29.0378	28.6631	28.8978	28.9873	29.3940
	SSIM↑	0.7773	0.7896	0.7667	0.7822	0.7734	0.7849	0.7907	0.8012	0.7910	0.7985	0.7882	0.7959	0.8026	0.8118
	LPIPS↓	0.1150	0.0995	0.1207	0.1143	0.1085	0.1021	0.1021	0.0974	0.0993	0.0952	0.0978	0.0936	0.0944	0.0911
	DISTS↓	0.0594	0.0518	0.0637	0.0610	0.0541	0.0510	0.0491	0.0522	0.0522	0.0519	0.0494	0.0499	0.0496	0.0490
Urban100	PSNR↑	24.3548	25.2991	24.4686	24.5959	24.7978	25.2672	25.2205	25.6060	25.4537	25.5851	25.5041	25.7764	25.8311	26.2520
	SSIM↑	0.7340	0.7606	0.7294	0.7366	0.7473	0.7573	0.7628	0.7696	0.7661	0.7705	0.7696	0.7761	0.7850	0.7929
	LPIPS↓	0.1234	0.1061	0.1381	0.1287	0.1186	0.1087	0.1094	0.1048	0.1084	0.1037	0.1053	0.1007	0.0998	0.0941
	DISTS↓	0.0879	0.0811	0.1044	0.1010	0.0850	0.0809	0.0797	0.0786	0.0793	0.0785	0.0805	0.0788	0.0807	0.0783
BSDS100	PSNR↑	25.3277	25.7504	25.4646	25.5562	25.5092	25.6818	25.7918	26.1428	25.9741	26.0676	25.7897	25.9174	26.1063	26.2676
	SSIM↑	0.6533	0.6723	0.6510	0.6598	0.6599	0.6649	0.6791	0.6849	0.6818	0.6870	0.6731	0.6768	0.6908	0.6957
	LPIPS↓	0.1601	0.1477	0.1736	0.1675	0.1602	0.1568	0.1505	0.1490	0.1534	0.1469	0.1492	0.1436	0.1574	0.1450
	DISTS↓	0.1173	0.1148	0.1280	0.1274	0.1186	0.1160	0.1137	0.1155	0.1175	0.1160	0.1113	0.1122	0.1168	0.1126
Manga109	PSNR↑	28.4125	29.2324	27.8481	28.2400	28.5608	28.9309	29.1934	29.7105	29.6204	29.7949	29.2020	29.4077	29.8802	30.2567
	SSIM↑	0.8595	0.8697	0.8497	0.8583	0.8591	0.8618	0.8754	0.8794	0.8734	0.8807	0.8698	0.8753	0.8892	0.8935
	LPIPS↓	0.0644	0.0566	0.0754	0.0690	0.0663	0.0622	0.0524	0.0520	0.0540	0.0502	0.0577	0.0532	0.0469	0.0440
	DISTS↓	0.0468	0.0403	0.0577	0.0564	0.0460	0.0454	0.0355	0.0378	0.0354	0.0353	0.0436	0.0429	0.0341	0.0345
General100	PSNR↑	29.4251	30.0092	29.1108	29.4338	29.4237	29.7783	29.9510	30.3979	30.2891	30.4594	29.9434	29.9606	30.4339	30.4839
	SSIM↑	0.8095	0.8215	0.8017	0.8122	0.8091	0.8160	0.8222	0.8317	0.8280	0.8330	0.8220	0.8230	0.8352	0.8370
	LPIPS↓	0.0878	0.0795	0.0954	0.0908	0.0863	0.0809	0.0780	0.0761	0.0800	0.0760	0.0768	0.0760	0.0765	0.0727
	DISTS↓	0.0877	0.0832	0.0977	0.0948	0.0890	0.0859	0.0801	0.0814	0.0806	0.0796	0.0817	0.0826	0.0824	0.0826

DM-based methods, we calculate the self-similarity graphs (SSG) of both ISR output and ground-truth (GT), and consequently introduce a self-similarity loss (SSL) between them to supervise the reconstruction of image details and structures.

3.1 Image Self-similarity

For a natural image, one can observe many repetitive patterns across it, known as the image self-similarity. Such a property has been used to improve the image restoration performance for a long time [3, 11]. Actually, the self-attention mechanism [44, 61] in transformer models exploits the image self-similarity in deep feature space. In this paper, we adopt the Exponential Euclidean distance [3] to calculate the self-similarity. For any two patches $I_p, I_q \in \mathbb{R}^{(2f+1) \times (2f+1) \times C}$ centered at pixels μ_p and μ_q in image $I \in \mathbb{R}^{H \times W \times C}$, respectively, where f denotes the patch radius, H , W and C are the image height, width and channel number ($C=3$ for RGB images), we firstly compute the squared Euclidean distance between I_p and I_q :

$$d^2(I_p, I_q) = \frac{1}{C(2f+1)^2} \sum_{i=1}^C \sum_{j=-f}^f (\mu_{p+j}^i - \mu_{q+j}^i)^2, \quad (1)$$

where μ_{p+j}^i and μ_{q+j}^i denote the neighborhood pixels around μ_p^i and μ_q^i in patch I_p and I_q , respectively. The similarity $S(I_p, I_q)$ between

I_p and I_q is calculated as:

$$S(I_p, I_q) = e^{-\frac{d^2(I_p, I_q)}{h}}, \quad (2)$$

where $h > 0$ is a scaling factor. One can see that $0 \leq S(I_p, I_q) \leq 1$. When the Euclidean distance $d^2(I_p, I_q)$ approaches to 0, the similarity $S(I_p, I_q)$ approaches to 1, indicating that the two patches are highly similar.

3.2 Mask Generation

By using the self-similarity measure defined in Eq. 2, we could compute the similarity of a patch with all the other patches in the whole image, and construct a self-similarity graph (SSG). However, this is computationally expensive because the size of such an SSG will be $H^2 \times W^2$. Actually, we do not need to calculate the self-similarity for each patch since the challenges of Real-ISR lie in edge and texture areas instead of smooth regions. Therefore, we can generate a mask of edge/texture pixels to indicate where we should calculate the SSG. For simplicity, we first generate an edge map $E \in \mathbb{R}^{H \times W}$ by applying the Laplacian operator, denoted by L , to the GT image $I_{HR} \in \mathbb{R}^{H \times W \times C}$, i.e., $E = L \otimes I_{HR}$. Then, we obtain the binary mask $M \in \mathbb{R}^{H \times W}$ by thresholding E :

$$M_{i,j} = \begin{cases} 0, & E_{i,j} \leq t \\ 1, & E_{i,j} > t \end{cases} \quad (3)$$

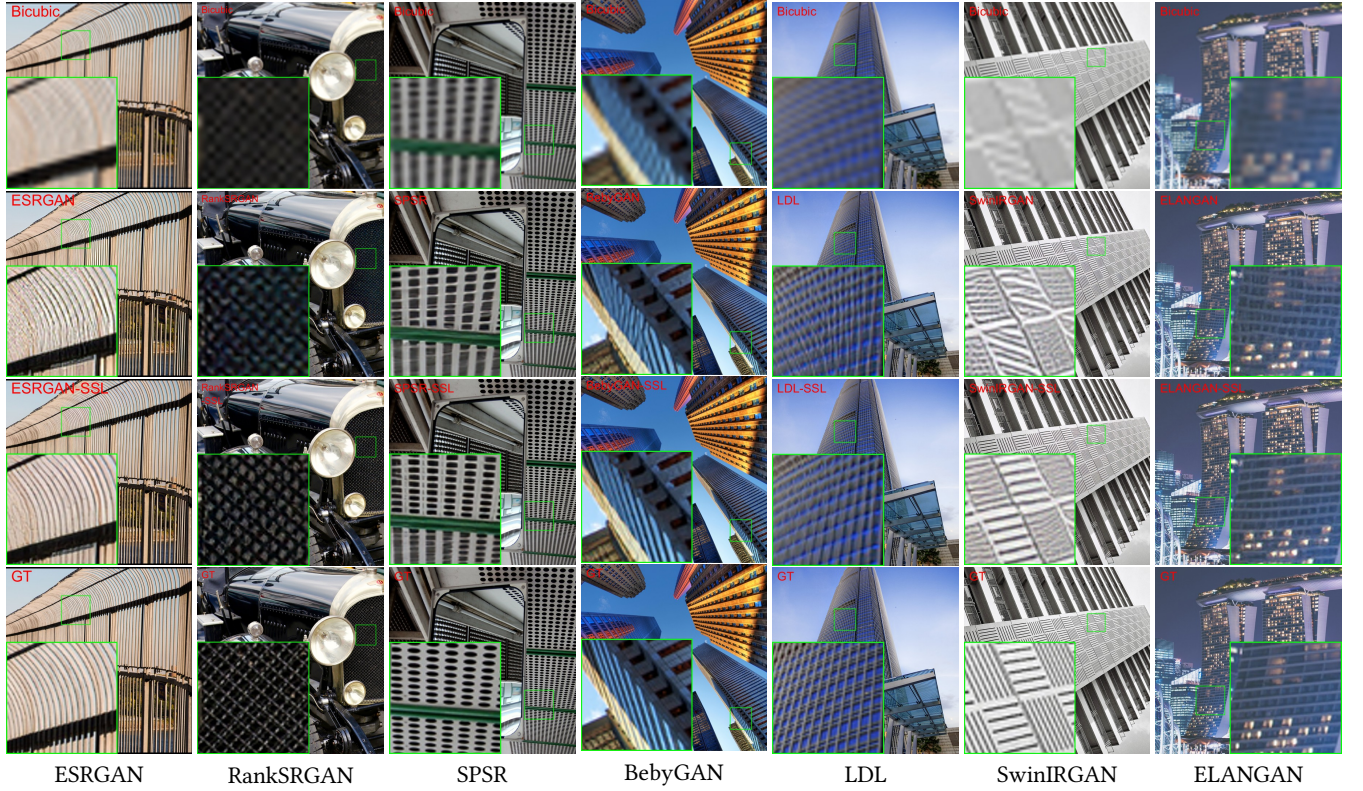


Figure 4: Visual comparison of the state-of-the-art GAN based Real-ISR models and their counterparts trained with our SSL. The bicubic degradation model is used here. From the top row to the bottom row are the results of bicubic interpolation, the original Real-ISR model, the Real-ISR model trained with our SSL, and the GT image. Please zoom in for better observation.

where t is a threshold. We empirically set it to 20 to retain most of the true edge pixels while filtering out smooth and trivial image features. M is computed in an off-line manner to avoid the repetitive computation in each iteration.

In the training progress, for pixels at (i, j) where $M_{i,j} = 1$, we find the corresponding RGB pixels μ_p in the GT image and the ISR output, and calculate their SSG for comparison. On the DF2K_OST training dataset, the edge pixels occupy only 13% of the total amount of image pixels. By using M to guide the construction of SSG, we can not only reduce significantly the training cost, but also concentrate on the image edges and textures.

3.3 Self-similarity Graph Calculation

For an edge pixel p in the original RGB image I (the corresponding pixel in the Mask M is $M_p = 1$), we define a search area $I_{K_s} \in \mathbb{R}^{K_s \times K_s \times C}$ as well as a local window $I_p \in \mathbb{R}^{K_w \times K_w \times C}$ centered at it, where $K_w = 2f + 1$ and f is the radius of the window. Then for each pixel q in the search area, we extract a sliding window $I_q \in \mathbb{R}^{K_w \times K_w \times C}$ to calculate its similarity with I_p , i.e., $S(I_p, I_q)$, by Eq. 1 and Eq. 2. Then we normalize $S(I_p, I_q)$ as:

$$\tilde{S}(I_p, I_q) = \frac{1}{\epsilon} * S(I_p, I_q), \quad (4)$$

where $\epsilon = \sum_{q \in I_{K_s}} S(I_p, I_q)$ is the normalization factor.

The overall calculation procedure of SSG is illustrated in Fig. 3. To be more specific, for each edge pixel in the mask, we find the corresponding pixels in the GT image and ISR image, and set a search area centred at them. Then we set a local sliding window to calculate the similarity between the patch centered at the central pixel and another patch centered at the pixels in the search area. All the values of $\tilde{S}(I_p, I_q)$ builds the SSG of image I , which describes the inherent structural similarity distribution of the image. In practice, we could sample I_q with a stride s to further reduce the computational cost (we set $s = 3$ in our implementation).

3.4 Self-similarity Loss

Denote by \tilde{S}_{HR} and \tilde{S}_{ISR} the SSG of the GT image and the ISR output, respectively. We can use their distance as the loss to supervise the network training. Here we employ the KL-divergence and L_1 distance to build the SSL:

$$L_{SSL} = D_{KL}(\tilde{S}_{HR} || \tilde{S}_{ISR}) + \alpha |\tilde{S}_{ISR} - \tilde{S}_{HR}|, \quad (5)$$

where α is a balance parameter and we simply set it as 1 in all our experiments.

SSL in GAN-based Models. To apply SSL into an off-the-shelf GAN-based Real-ISR method, we just need to add the above L_{SSL} loss to its original loss function $L_{original}$ (e.g. pixel-wise L_1 loss,

Table 2: Quantitative results of three representative DM-based Real-ISR models and their counterparts coupled with the proposed SSL. For each of the three groups of comparisons, the better results are highlighted in boldface. The PSNR and SSIM indices are computed in the Y channel of Ycbr space.

Method		StableSR	StableSR-SSL	ResShift	ResShif-SSL	DiffIR	DiffIR-SSL
Training Dataset		DF2K_OST+DIV8K+FFHQ					
DIV2K100	PSNR↑	23.2988	23.1111	23.6136	24.7275	25.5008	25.4124
	SSIM↑	0.5654	0.5203	0.5701	0.6161	0.6570	0.6470
	LPIPS↓	0.3125	0.3588	0.3712	0.3417	0.2651	0.2664
	DISTS↓	0.2045	0.2323	0.2379	0.2236	0.2013	0.1977
	FID↓	24.4578	28.0564	49.3542	35.4661	25.7638	26.1045
	NIQE↓	4.7806	4.5219	6.2656	6.6347	5.1936	4.9569
	CLIP-IQA↑	0.6694	0.6940	0.6859	0.5343	0.5130	0.5262
	MUSIQ↑	65.7710	67.7485	64.0147	57.1369	58.5725	60.8936
DRealSR	PSNR↑	28.1526	27.6065	27.5799	29.4468	29.9046	29.5164
	SSIM↑	0.7529	0.6736	0.7364	0.7975	0.8188	0.8171
	LPIPS↓	0.3315	0.4312	0.3941	0.3818	0.2895	0.2683
	DISTS↓	0.2263	0.2810	0.2709	0.2684	0.2118	0.2031
	FID↓	151.1807	156.5795	180.2996	161.8707	141.2654	141.9467
	NIQE↓	6.5808	6.2259	7.0837	9.0121	7.1668	7.5738
	CLIP-IQA↑	0.6207	0.6103	0.6490	0.3922	0.3191	0.3722
	MUSIQ↑	58.4207	60.5404	58.4495	38.3946	41.9419	45.0333
RealSR	PSNR↑	24.7021	25.3236	25.5153	26.6132	27.4546	26.9851
	SSIM↑	0.7065	0.6563	0.7024	0.7493	0.7848	0.7847
	LPIPS↓	0.3018	0.3744	0.3759	0.3446	0.2538	0.2411
	DISTS↓	0.2135	0.2496	0.2725	0.2552	0.1928	0.1892
	FID↓	129.5313	131.4425	164.7055	149.3277	117.8279	119.3884
	NIQE↓	5.9430	5.1812	6.3815	7.0816	6.4811	6.2603
	CLIP-IQA↑	0.6178	0.6324	0.6838	0.4760	0.3437	0.3677
	MUSIQ↑	65.7834	65.6814	63.2059	52.8008	52.0040	54.8398
DPED-iPhone	NIQE↓	6.7597	6.1154	8.9634	9.4691	7.2465	7.1488
	CLIP-IQA↑	0.4694	0.4944	0.6174	0.4109	0.2664	0.3045
	MUSIQ↑	50.6582	53.7349	47.8474	37.6449	36.4193	41.2825

perceptual loss and GAN loss), and then re-train the model:

$$L_{total} = L_{original} + \beta L_{SSL}, \quad (6)$$

where β is a balance parameter.

SSL in DM-based Models. As for those latent DM-based Real-ISR methods, StableSR [63] and ResShift [79], the $L_{original}$ is applied to predict the desired noise in latent space. Since SSL is computed in image space, we need to pass the predicted noise through the VAE decoder to output the ISR image, as shown in Fig. 2(b), and then apply the SSL to the reconstructed image. We also employ a pixel-wise L_1 loss for more stable training. The total loss is:

$$L_{total} = L_{original} + \beta L_{SSL} + \gamma L_1, \quad (7)$$

where β, γ are balance parameters. The L_{SSL} and L_1 will back-propagate their gradients to update the parameters of the denoising UNet and the controlling parts in DMs.

4 Experimental Results

4.1 Experiments on GAN-based Models

Comparison Methods. Our proposed SSL can be directly applied to the existing GAN-based Real-ISR models with either simple

bicubic degradation or complex mixture degradations [65, 84] as a plug-and-play module to improve their performance. For bicubic degradation, we embed SSL into ESRGAN [67], RankSRGAN [87], SPSR [46], BebyGAN [35] and LDL [41]. For complex mixture degradations, we embed SSL into Real-ESRGAN [65] and BSRGAN [84]. Most of the above models employ the CNN backbone (e.g., RRDB [67] or SRResNet [33]) as the generator. In this paper, we also employ the transformer backbones, i.e., SwinIR [40] and ELAN [89], as the generator, resulting in the SwinIRGAN and ELANGAN models. For each of the above Real-ISR models (e.g., ESRGAN), we denote by “*-SSL” (e.g., ESRGAN-SSL).

Training Details. For each of the evaluated Real-ISR methods, we train its SSL guided counterpart with the same patch size and training dataset (i.e., DIV2K [60], DF2K [1, 60] and DF2K-OST [1, 60, 66]) as the original method. In the experiments with complex degradations, since the original degradation setting in Real-ESRGAN and BSRGAN is too heavy, we follow the Real-ESRGAN and BSRGAN settings in HGGT [6] (which has weaker degradation level) for training data generation. The Adam [32] optimizer is adopted. The initial learning rate is set to $1e-4$, which is halved after 200K iterations for CNN backbones, and 200K, 250K, 275K, 287.5K



Figure 5: Visual comparison of the state-of-the-art DM based Real-ISR models and their counterparts trained with our SSL. From the top row to the bottom row are the results of bicubic interpolation, the original Real-ISR model, the Real-ISR model trained with our SSL, and the GT image. Please zoom in for better observation.

iterations for transformer backbones. When calculating SSG, the search area I_{K_s} is set to 25, the sliding window I_{K_w} is set to 9, and the scaling factor h is set to 0.004. β is set to 1000. All experiments are conducted on NVIDIA RTX 3090 GPUs. All of the SSL guided models are fine-tuned from a well-trained fidelity-oriented version (e.g. RRDB [67], SwinIR [40] or ELAN [89]) which is trained only with $L1$ loss without a discriminator for better initialization.

Evaluation Datasets and Metrics. We employ the widely-used testing benchmarks, including Set5 [2], Set14 [81], DIV2K100 [60], Urban100 [26], BSDS100 [47], Manga109 [48], General100 [14], to evaluate the competing methods. Considering the fact that there is certain randomness in the synthesis of LR images when using the complex mixture degradation models in [65, 84], for each test image, we synthesize a group of 30 LR images using randomly sampled degradation factors, and report the averaged metrics for fair and solid evaluation. We compute PSNR and SSIM [68] in the Y channel for fidelity measurement. For perceptual quality, LPIPS [86] and DISTS [12] are used for quantitative assessment.

Results for Bicubic Degradation. Table 1 shows the quantitative results of different Real-ISR models when bicubic degradation is used. It can be seen that on all the 7 testing datasets, our SSL

guided models surpass their original counterparts in most of the fidelity (PSNR, SSIM) and perceptual (LPIPS, DISTS) measures, no matter the CNN or transformer backbones are used. This demonstrates that the image SSG could characterize the image inherent structures, and our SSL could provide effective supervision in the Real-ISR model training process, enforcing the models to hallucinate more correct contents with better fidelity and suppressing the visual artifacts to achieve better perceptual quality. It is worth mentioning that our SSL will not introduce any extra cost in the inference process.

Qualitative Result. Fig. 4 provides visual comparisons between major Real-ISR models and their SSL-guided version in the case of bicubic degradation. One can clearly see that the SSL-guided models could generate clearer textures (the 1st column), or richer details (the 2nd column) and correct the twisted textures (the 3rd/4th/5th/6th/7th columns) generated by the original models. Such observations echo with the results in Table 1, proving again that SSL could hallucinate correct details and suppress artifacts.

Results for Complex Degradation. Due to the page limit, we provide the quantitative results of GAN-based Real-ISR models and their SSL guided versions under complex image degradation, as

well as the visualization comparisons between them, in the **supplementary material**.

4.2 Experiments on DM-based Models

Comparison Methods. We embed SSL into three representative DM-based models, including StableSR [62], ResShift [79] and DiffIR [72]. For each of the above Real-ISR models (e.g., StableSR), we denote by “*-SSL” (StableSR-SSL).

Training Details. For each of the evaluated DM-based Real-ISR method, we employ the same training datasets (including DF2K-OST [1, 60, 66], DIV8K [20], FFHQ [29]), and apply the same degradation pipeline as that used in StableSR [62]. The training patch size and iterations in SSL-guided versions are set to the same as the original method. The Adam [32] optimizer is used. The learning rate is fixed to $5e-5$. When calculating SSG, the search area I_{K_s} is set to 25, the sliding window I_{K_w} is set to 9, and the scaling factor h is set to 0.004. For SSL guided StableSR and DiffIR, the weight β and γ in Eq. 7 are set to 1 and 0.1, respectively. For SSL guided DiffIR, since the original model [72] already utilizes pixel-wise $L1$ loss, then we implement the loss function type as Eq. 6, β is set to 1000. All experiments are conducted on NVIDIA V100 GPUs. We update all of the parameters of UNet in the pre-trained DM as well as the controlling parts towards the SSL-guided counterparts.

Evaluation Datasets and Metrics. We utilize the testing images from StableSR [62], including the 3000 synthesized DIV2K100 low-quality testing images (each GT image has a group of 30 LR images generated from DIV2K100 [60] dataset with complicated degradation factors), RealSR [4] (100 real-world low-quality images with their corresponding GTs obtained by cameras), DRealSR [70] (93 real-world low-quality images with their corresponding GTs captured by cameras), DPED-iphone [28] (113 real-world low-quality images taken by iPhone without GT). We compute full-reference image quality metrics, including PSNR, SSIM [68], LPIPS [86] and DISTs [12], and no-reference image quality metrics, including NIQE [50], CLIP-IQA [62] and MUSIQ [30]. The statistical distance metric FID [24] is also calculated.

Quantitative Result. Tab. 2 shows the numerical results of the original DM-based Real-ISR methods and their SSL guided versions. One can see that StableSR-SSL obtains better no-reference metrics (NIQE/CLIP-IQA/MUSIQ) while gets worse full-reference metrics (PSNR/SSIM/LPIPS/DISTs). ResShift-SSL gets better full-reference metrics (PSNR/SSIM/LPIPS/DISTs) but worse no-reference metrics (NIQE/CLIP-IQA/MUSIQ). DiffIR-SSL gets better perceptual-relevant metrics (LPIPS/DISTs/NIQE/CLIP-IQA/MUSIQ). While different SSL guided models obtain different performance, it is still reasonable for the following reasons: (1). StableSR-SSL leverages a pretrained Stable-Diffusion model [55], which is trained on LAION-5B [57], a multi-modal dataset that contains a vast number of text-to-image pairs. This results in a distinct data distribution divergence when compared to the general training datasets used for SR tasks, such as DF2K [1, 60] and DIV8K [20]. Consequently, during inference stage, the results generated by StableSR-SSL, exhibit a notable difference from the GT in the test set (such as DIV2K100). Thus all full-reference metrics get failure, while get much better no-reference metrics, which also indicate better perception quality. (2) ResShift-SSL gets better FR-IQA (PSNR/SSIM/LPIPS/DISTs/FID)

results, this indicated that SSL could help ResShift reconstruct textures with higher fidelity. As for the worse NR-IQA metrics, this is mainly because the existing NR-IQA metrics, including NIQE, CLIP-IQA and MUSIQ, favor the images with more high-frequency details, even these details are wrong. As can be seen from Fig. 6 in the **supplementary**, ResShift hallucinates many wrong details (e.g., on the windows in column 1), while ResShift-SSL successfully removes those artifacts. Our user study in Fig. ?? also showed that 73.07% of the observers pick the results of ResShift-SSL. However, the NR-IQA metrics prefer the results of ResShift because they are not accurate enough to represent the human perception yet. (3). DiffIR-SSL not only trains a latent-diffusion model from scratch, but also utilizes a discriminator. Due to the influence introduced by the discriminator, the PSNR/SSIM just get worse, but obtains better perception-relevant metrics (LPIPS/DISTs/NIQE/CLIP-IQA/MUSIQ).

Qualitative Result. Fig. 5 shows the visualization results. One can see that compared with the original DM-based Real-ISR methods, their SSL guided versions perform significantly better in restoring the image structures and details, demonstrating the strong structure regularization capability of SSL. For example, StableSR generates false patterns in the T-shirt (column 1) and incomplete details on the peristyle (column 2), while the SSL guided StableSR restores correct T-shirt pattern and hallucinates more complete structures on peristyle. For ResShift, it either over-smooths the details (column 3) or generate wrong textures (column 4), while SSL can help to solve this issue. Similar observations go to DiffIR. All these results validate the effectiveness of SSL in encouraging the Real-ISR model to generate more delicate details. More visual comparisons that validate the perception improvement of SSL can be found in the **supplementary material**.

Due to the limited pages, we also provide the following contents in our **supplementary material**: (1). A user study to validate the performance of SSL. (2). The training cost analysis towards SSL. (3). Ablation studies about the selection of hyper-parameters, such as K_s , K_w , β in Eq. 6 and Eq. 7. (4). Limitation of SSL.

5 Conclusion

Generative image super-resolution methods, including GAN-based and DM-based ones, are prone to generating visual artifacts. In this work, we proposed a novel use of the image self-similarity prior for improving the generative real-world image super-resolution results. Specifically, we explicitly computed the self-similarity graph (SSG) of the image, and took the difference between the SSG maps of ground-truth image and Real-ISR output as a self-similarity loss (SSL) to supervise the network training. SSL could be easily embedded in off-the-shelf Real-ISR models, including GAN-based and DM-based ones, as a plug-and-play penalty, guiding the model to more stably generate realistic details and suppress false generations and visual artifacts. Our extensive experiments on benchmark datasets validated the generality and effectiveness of the proposed SSL in generative Real-ISR tasks.

Acknowledgments

We faithfully thank PolyU-OPPO Joint Innovation Lab for supporting our projects.

References

- [1] Eirikur Agustsson and Radu Timofte. 2017. NTIRE 2017 Challenge on Single Image Super-resolution: Dataset and study. In *IEEE Conference on Computer Vision and Pattern Recognition Workshop*. IEEE, 126–135.
- [2] Marco Bevilacqua, Aline Roumy, Christine Guillemot, and Marie Line Alberi-Morel. 2012. Low-complexity Single-image Super-resolution Based on Nonnegative Neighbor Embedding. In *British Machine Vision Conference*. 135.1–135.10.
- [3] Antoni Buades, Bartomeu Coll, and Jean-Michel Morel. 2011. Non-local means denoising. *Image Processing On Line* 1 (2011), 208–212.
- [4] Jianrui Cai, Hui Zeng, Hongwei Yong, Zisheng Cao, and Lei Zhang. 2019. Toward Real-world Single Image Super-resolution: A New Benchmark and a New Model. In *International Conference on Computer Vision*. IEEE, 3086–3095.
- [5] Chang Chen, Zhiwei Xiong, Xinmei Tian, Zheng-Jun Zha, and Feng Wu. 2019. Camera Lens Super-resolution. In *IEEE Conference on Computer Vision and Pattern Recognition*. IEEE, 1652–1660.
- [6] Du Chen, Jie Liang, Xindong Zhang, Ming Liu, Hui Zeng, and Lei Zhang. 2023. Human guided ground-truth generation for realistic image super-resolution. In *IEEE Conference on Computer Vision and Pattern Recognition*. IEEE, 14082–14091.
- [7] Hao-Wei Chen, Yu-Syuan Xu, Min-Fong Hong, Yi-Min Tsai, Hsien-Kai Kuo, and Chun-Yi Lee. 2023. Cascaded Local Implicit Transformer for Arbitrary-Scale Super-Resolution. In *IEEE Conference on Computer Vision and Pattern Recognition*. IEEE, 18257–18267.
- [8] Xiangyu Chen, Xintao Wang, Jiantao Zhou, Yu Qiao, and Chao Dong. 2023. Activating more pixels in image super-resolution transformer. In *IEEE Conference on Computer Vision and Pattern Recognition*. IEEE, 22367–22377.
- [9] Haram Choi, Jeongmin Lee, and Jihoon Yang. 2023. N-gram in swin transformers for efficient lightweight image super-resolution. In *IEEE Conference on Computer Vision and Pattern Recognition*. IEEE, 2071–2081.
- [10] Victor Cornillere, Abdelaziz Djelouah, Wang Yifan, Olga Sorkine-Hornung, and Christopher Schroers. 2019. Blind Image Super-resolution with Spatially Variant Degradations. *ACM Transactions on Graphics* 38, 6 (2019), 1–13.
- [11] Kostadin Dabov, Alessandro Foi, Vladimir Katkovnik, and Karen Egiazarian. 2007. Image denoising by sparse 3-D transform-domain collaborative filtering. *IEEE Transactions on Image Processing* 16, 8 (2007), 2080–2095.
- [12] Keyan Ding, Kede Ma, Shiqi Wang, and Eero P Simoncelli. 2020. Image Quality Assessment: Unifying Structure and Texture Similarity. *IEEE Transactions on Pattern Analysis and Machine Intelligence* 44, 5 (2020), 2567–2581.
- [13] Chao Dong, Chen Change Loy, Kaiming He, and Xiaoou Tang. 2014. Learning a Deep Convolutional Network for Image Super-resolution. In *European Conference on Computer Vision*. Springer, 184–199.
- [14] Chao Dong, Chen Change Loy, and Xiaoou Tang. 2016. Accelerating the Super-resolution Convolutional Neural Network. In *European Conference on Computer Vision*. Springer, 391–407.
- [15] Weisheng Dong, Lei Zhang, Guangming Shi, and Xin Li. 2012. Nonlocally centralized sparse representation for image restoration. *IEEE transactions on Image Processing* 22 (2012), 1620–1630.
- [16] Chen Du, He Zewei, Sun Anshun, Yang Jiangxin, Cao Yanlong, Cao Yanpeng, Tang Siliang, and Michael Ying Yang. 2019. Orientation-aware deep neural network for real image super-resolution. In *Proceedings of the IEEE/CVF Conference on Computer Vision and Pattern Recognition Workshops*. 0–0.
- [17] Garas Gendy, Nabil Sabor, Jingchao Hou, and Guanghui He. 2023. A Simple Transformer-Style Network for Lightweight Image Super-Resolution. In *IEEE Conference on Computer Vision and Pattern Recognition*. 1484–1494.
- [18] Ian Goodfellow, Jean Pouget-Abadie, Mehdi Mirza, Bing Xu, David Warde-Farley, Sherjil Ozair, Aaron Courville, and Yoshua Bengio. 2020. Generative Adversarial Networks. *Commun. ACM* 63, 11 (2020), 139–144.
- [19] Jinjin Gu, Hannan Lu, Wangmeng Zuo, and Chao Dong. 2019. Blind Super-resolution with Iterative Kernel Correction. In *IEEE Conference on Computer Vision and Pattern Recognition*. 1604–1613.
- [20] Shuhang Gu, Andreas Lugmayr, Martin Danelljan, Manuel Fritsche, Julien Lamour, and Radu Timofte. 2019. Div8k: Diverse 8k resolution image dataset. In *2019 IEEE/CVF International Conference on Computer Vision Workshop (ICCVW)*. IEEE, 3512–3516.
- [21] Shuhang Gu, Lei Zhang, Wangmeng Zuo, and Xiangchu Feng. 2014. Weighted nuclear norm minimization with application to image denoising. In *IEEE Conference on Computer Vision and Pattern Recognition*. 2862–2869.
- [22] Xiangyu He, Zitao Mo, Peisong Wang, Yang Liu, Mingyuan Yang, and Jian Cheng. 2019. Ode-inspired Network Design for Single Image super-resolution. In *IEEE Conference on Computer Vision and Pattern Recognition*. 1732–1741.
- [23] Zewei He, Du Chen, Yanpeng Cao, Jiangxin Yang, Yanlong Cao, Xin Li, Siliang Tang, Yueting Zhuang, and Zheming Lu. 2022. Single Image Super-Resolution Based on Progressive Fusion of Orientation-aware Features. *Pattern Recognition* (2022), 109038.
- [24] Martin Heusel, Hubert Ramsauer, Thomas Unterthiner, Bernhard Nessler, and Sepp Hochreiter. 2017. Gans Trained by a Two Time-scale Update Rule Converge to a Local Nash Equilibrium. *Advances in Neural Information Processing Systems* 30 (2017).
- [25] Jonathan Ho, Ajay Jain, and Pieter Abbeel. 2020. Denoising diffusion probabilistic models. *Advances in Neural Information Processing Systems* 33 (2020), 6840–6851.
- [26] Jia-Bin Huang, Abhishek Singh, and Narendra Ahuja. 2015. Single Image super-resolution from Transformed Self-exemplars. In *IEEE Conference on Computer Vision and Pattern Recognition*. 5197–5206.
- [27] Yawen Huang, Ling Shao, and Alejandro F Frangi. 2017. Simultaneous super-resolution and cross-modality synthesis of 3D medical images using weakly-supervised joint convolutional sparse coding. In *IEEE Conference on Computer Vision and Pattern Recognition*. 6070–6079.
- [28] Andrey Ignatov, Nikolay Kobyshev, Radu Timofte, Kenneth Vanhoey, and Luc Van Gool. [n. d.]. DSLR-quality Photos on Mobile Devices with Deep Convolutional Networks. In *Proc. IEEE*.
- [29] Tero Karras, Samuli Laine, and Timo Aila. 2019. A style-based generator architecture for generative adversarial networks. In *Proceedings of the IEEE/CVF conference on computer vision and pattern recognition*. 4401–4410.
- [30] Junjie Ke, Qifei Wang, Yilin Wang, Peyman Milanfar, and Feng Yang. 2021. Musiq: Multi-scale image quality transformer. In *Proceedings of the IEEE/CVF International Conference on Computer Vision*. 5148–5157.
- [31] Jiwon Kim, Jung Kwon Lee, and Kyoung Mu Lee. 2016. Accurate Image Super-resolution Using Very Deep Convolutional Networks. In *IEEE Conference on Computer Vision and Pattern Recognition*. 1646–1654.
- [32] Diederik P Kingma and Jimmy Ba. 2014. Adam: A method for stochastic optimization. *arXiv preprint arXiv:1412.6980* (2014).
- [33] Christian Ledig, Lucas Theis, Ferenc Huszar, Jose Caballero, Andrew Cunningham, Alejandro Acosta, Andrew Aitken, Alykhan Tejani, Johannes Totz, Zehan Wang, et al. 2017. Photo-realistic Single Image Super-resolution Using a Generative Adversarial Network. In *IEEE Conference on Computer Vision and Pattern Recognition*. 4681–4690.
- [34] Sen Lei, Zhenwei Shi, and Zhengxia Zou. 2017. Super-resolution for remote sensing images via local-global combined network. *IEEE Geoscience and Remote Sensing Letters* 14, 8 (2017), 1243–1247.
- [35] Wenbo Li, Kun Zhou, Lu Qi, Liying Lu, and Jiangbo Lu. 2022. Best-buddy gans for highly detailed image super-resolution. In *Proceedings of the AAAI Conference on Artificial Intelligence*. 1412–1420.
- [36] Xiaoming Li, Chaofeng Chen, Xianhui Lin, Wangmeng Zuo, and Lei Zhang. 2022. From face to natural image: Learning real degradation for blind image super-resolution. In *European Conference on Computer Vision*. Springer, 376–392.
- [37] Xiaoming Li, Shiguang Zhang, Shangchen Zhou, Lei Zhang, and Wangmeng Zuo. 2022. Learning Dual Memory Dictionaries for Blind Face Restoration. *IEEE Transactions on Pattern Analysis and Machine Intelligence* 45, 5 (2022), 5904–5917.
- [38] Xiaoming Li, Wangmeng Zuo, and Chen Change Loy. 2023. Learning Generative Structure Prior for Blind Text Image Super-Resolution. In *Proceedings of the IEEE/CVF Conference on Computer Vision and Pattern Recognition*. 10103–10113.
- [39] Zhen Li, Jinglei Yang, Zheng Liu, Xiaomin Yang, Gwanggil Jeon, and Wei Wu. 2019. Feedback network for image super-resolution. In *IEEE Conference on Computer Vision and Pattern Recognition*. 3867–3876.
- [40] Jingyun Liang, Jiezhang Cao, Guolei Sun, Kai Zhang, Luc Van Gool, and Radu Timofte. 2021. SwinIR: Image Restoration Using Swin Transformer. In *Proceedings of the IEEE/CVF International Conference on Computer Vision Workshop*. 1833–1844.
- [41] Jie Liang, Hui Zeng, and Lei Zhang. 2022. Details or Artifacts: A Locally Discriminative Learning Approach to Realistic Image Super-Resolution. In *IEEE Conference on Computer Vision and Pattern Recognition*. 5657–5666.
- [42] Bee Lim, Sanghyun Son, Heewon Kim, Seungjun Nah, and Kyoung Mu Lee. 2017. Enhanced Deep Residual Networks for Single Image Super-resolution. In *IEEE Conference on Computer Vision and Pattern Recognition Workshop*. 136–144.
- [43] Xinqi Lin, Jingwen He, Ziyang Chen, Zhaoyang Lyu, Ben Fei, Bo Dai, Wanli Ouyang, Yu Qiao, and Chao Dong. 2023. DiffBIR: Towards Blind Image Restoration with Generative Diffusion Prior. *arXiv preprint arXiv:2308.15070* (2023).
- [44] Ze Liu, Yutong Lin, Yue Cao, Han Hu, Yixuan Wei, Zheng Zhang, Stephen Lin, and Baining Guo. 2021. Swin transformer: Hierarchical vision transformer using shifted windows. In *Proceedings of the IEEE/CVF international conference on computer vision*. 10012–10022.
- [45] Zhengxiong Luo, Yan Huang, Shang Li, Liang Wang, and Tieniu Tan. 2022. Learning the degradation distribution for blind image super-resolution. In *Proceedings of the IEEE/CVF Conference on Computer Vision and Pattern Recognition*. 6063–6072.
- [46] Cheng Ma, Yongming Rao, Yean Cheng, Ce Chen, Jiwen Lu, and Jie Zhou. 2020. Structure-preserving super resolution with gradient guidance. In *Proceedings of the IEEE/CVF conference on computer vision and pattern recognition*. 7769–7778.
- [47] David Martin, Charles Fowlkes, Doron Tal, and Jitendra Malik. [n. d.]. A Database of Human Segmented Natural Images and its Application to Evaluating Segmentation Algorithms and Measuring Ecological Statistics. In *Proc. IEEE*.
- [48] Yusuke Matsui, Kota Ito, Yuji Aramaki, Azuma Fujimoto, Toru Ogawa, Toshihiko Yamasaki, and Kiyoharu Aizawa. 2017. Sketch-based Manga Etrieval Using Manga109 Dataset. *Multimedia Tools and Applications* 76, 20 (2017), 21811–21838.
- [49] Yiqun Mei, Yuchen Fan, and Yuqian Zhou. 2021. Image super-resolution with non-local sparse attention. In *IEEE Conference on Computer Vision and Pattern*

- Recognition. 3517–3526.
- [50] Anish Mittal, Rajiv Soundararajan, and Alan C Bovik. 2012. Making a “Completely Blind” Image Quality Analyzer. *IEEE Signal Processing Letters* 20, 3 (2012), 209–212.
 - [51] Ben Niu, Weilei Wen, Wenqi Ren, Xiangde Zhang, Lianping Yang, Shuzhen Wang, Kaihao Zhang, Xiaochun Cao, and Haifeng Shen. 2020. Single Image Super-resolution via a Holistic Attention Network. In *European Conference on Computer Vision*. Springer, 191–207.
 - [52] Joonkyu Park, Sanghyun Son, and Kyoung Mu Lee. 2023. Content-Aware Local GAN for Photo-Realistic Super-Resolution. In *Proceedings of the IEEE/CVF International Conference on Computer Vision*. 10585–10594.
 - [53] Seobin Park, Dongjin Kim, Sungyong Baik, and Tae Hyun Kim. 2023. Learning Controllable Degradation for Real-World Super-Resolution via Constrained Flows. *Proceedings of the International Conference on Machine Learning* (2023).
 - [54] Mohammad Saeed Rad, Behzad Bozorgtabar, Urs-Viktor Marti, Max Basler, Hazim Kemal Ekenel, and Jean-Philippe Thiran. 2019. Srobb: Targeted Perceptual Loss for Single Image Super-resolution. In *International Conference on Computer Vision*. 2710–2719.
 - [55] Robin Rombach, Andreas Blattmann, Dominik Lorenz, Patrick Esser, and Björn Ommer. 2022. High-resolution image synthesis with latent diffusion models. In *Proceedings of the IEEE/CVF Conference on Computer Vision and Pattern Recognition*. 10684–10695.
 - [56] Chitwan Saharia, Jonathan Ho, William Chan, Tim Salimans, David J Fleet, and Mohammad Norouzi. 2022. Image Super-resolution via Iterative Refinement. *IEEE Transactions on Pattern Analysis and Machine Intelligence* 45, 4 (2022), 4713–4726.
 - [57] Christoph Schuhmann, Romain Beaumont, Richard Vencu, Cade Gordon, Ross Wightman, Mehdi Cherti, Theo Coombes, Aarush Katta, Clayton Mullis, Mitchell Wortsman, et al. 2022. LAION-5B: An Open Large-scale Dataset for Training Next Generation Image-text Models. *Advances in Neural Information Processing Systems* 35 (2022), 25278–25294.
 - [58] Karen Simonyan and Andrew Zisserman. 2014. Very Deep Convolutional Networks for Large-scale Image Recognition. *arXiv preprint arXiv:1409.1556* (2014).
 - [59] Jiaming Song, Chenlin Meng, and Stefano Ermon. 2020. Denoising Diffusion Implicit Models. In *International Conference on Learning Representations*.
 - [60] Radu Timofte, Eirikur Agustsson, Luc Van Gool, Ming-Hsuan Yang, and Lei Zhang. 2017. NTIRE 2017 Challenge on Single Image Super-resolution: Methods and Results. In *IEEE Conference on Computer Vision and Pattern Recognition Workshop*. 114–125.
 - [61] Ashish Vaswani, Noam Shazeer, Niki Parmar, Jakob Uszkoreit, Llion Jones, Aidan N Gomez, Łukasz Kaiser, and Illia Polosukhin. 2017. Attention is All You Need. *Conference and Workshop on Neural Information Processing Systems* 30 (2017).
 - [62] Jianyi Wang, Kelvin CK Chan, and Chen Change Loy. 2023. Exploring clip for assessing the look and feel of images. In *Proceedings of the AAAI Conference on Artificial Intelligence*. 2555–2563.
 - [63] Jianyi Wang, Zongsheng Yue, Shangchen Zhou, Kelvin CK Chan, and Chen Change Loy. 2023. Exploiting Diffusion Prior for Real-World Image Super-Resolution. *arXiv preprint arXiv:2305.07015* (2023).
 - [64] Longguang Wang, Yingqian Wang, Xiaoyu Dong, Qingyu Xu, Jungang Yang, Wei An, and Yulan Guo. 2021. Unsupervised Degradation Representation Learning for Blind Super-resolution. In *IEEE Conference on Computer Vision and Pattern Recognition*. 10581–10590.
 - [65] Xintao Wang, Liangbin Xie, Chao Dong, and Ying Shan. [n. d.]. Real-ESRGAN: Training Real-world Blind Super-resolution with Pure Synthetic Data. In *Proc. IEEE*.
 - [66] Xintao Wang, Ke Yu, Chao Dong, and Chen Change Loy. 2018. Recovering Realistic Texture in Image Super-resolution by Deep Spatial Feature Transform. In *IEEE Conference on Computer Vision and Pattern Recognition*. 606–615.
 - [67] Xintao Wang, Ke Yu, Shixiang Wu, Jinjin Gu, Yihao Liu, Chao Dong, Yu Qiao, and Chen Change Loy. 2018. ESRGAN: Enhanced Super-resolution Generative Adversarial Networks. In *European Conference on Computer Vision Workshop*. 0–0.
 - [68] Zhou Wang, Alan C Bovik, Hamid R Sheikh, and Eero P Simoncelli. 2004. Image Quality Assessment: From Error Visibility to Structural Similarity. *IEEE Transactions on Image Processing* 13, 4 (2004), 600–612.
 - [69] Pengxu Wei, Yujing Sun, Xingbei Guo, Chang Liu, Guanbin Li, Jie Chen, Xiangyang Ji, and Liang Lin. 2023. Towards Real-World Burst Image Super-Resolution: Benchmark and Method. In *Proceedings of the IEEE/CVF International Conference on Computer Vision*. 13233–13242.
 - [70] Pengxu Wei, Ziwei Xie, Hannan Lu, Zongyuan Zhan, Qixiang Ye, Wangmeng Zuo, and Liang Lin. 2020. Component Divide-and-conquer for Real-world Image Super-resolution. In *European Conference on Computer Vision*. Springer, 101–117.
 - [71] Yunxuan Wei, Shuhang Gu, Yawei Li, Radu Timofte, Longcun Jin, and Hengjie Song. 2021. Unsupervised real-world image super resolution via domain-distance aware training. In *Proceedings of the IEEE/CVF Conference on Computer Vision and Pattern Recognition*. 13385–13394.
 - [72] Bin Xia, Yulun Zhang, Shiyin Wang, Yitong Wang, Xinglong Wu, Yapeng Tian, Wenming Yang, and Luc Van Gool. 2023. Diffir: Efficient Diffusion Model for Image Restoration. *Proceedings of the IEEE/CVF International Conference on Computer Vision* (2023).
 - [73] Liangbin Xie, Xintao Wang, Xiangyu Chen, Gen Li, Ying Shan, Jiantao Zhou, and Chao Dong. 2023. DeSRA: Detect and Delete the Artifacts of GAN-based Real-World Super-Resolution Models. *Proceedings of the International Conference on Machine Learning* (2023).
 - [74] Ruikang Xu, Mingde Yao, and Zhiwei Xiong. 2023. Zero-Shot Dual-Lens Super-Resolution. In *Proceedings of the IEEE/CVF Conference on Computer Vision and Pattern Recognition*. 9130–9139.
 - [75] Xiaoqian Xu, Pengxu Wei, Weikai Chen, Yang Liu, Mingzhi Mao, Liang Lin, and Guanbin Li. 2022. Dual adversarial adaptation for cross-device real-world image super-resolution. In *Proceedings of the IEEE/CVF Conference on Computer Vision and Pattern Recognition*. 5667–5676.
 - [76] Tao Yang, Peiran Ren, Xuansong Xie, and Lei Zhang. 2023. Pixel-Aware Stable Diffusion for Realistic Image Super-resolution and Personalized Stylization. *arXiv preprint arXiv:2308.14469* (2023).
 - [77] Zhicun Yin, Ming Liu, Xiaoming Li, Hui Yang, Longan Xiao, and Wangmeng Zuo. 2023. MetaF2N: Blind Image Super-Resolution by Learning Efficient Model Adaptation from Faces. In *Proceedings of the IEEE/CVF International Conference on Computer Vision*. 13033–13044.
 - [78] Jinsu Yoo, Taehoon Kim, Sihaeng Lee, Seung Hwan Kim, Honglak Lee, and Tae Hyun Kim. 2023. Enriched cnn-transformer feature aggregation networks for super-resolution. In *Proceedings of the IEEE/CVF Winter Conference on Applications of Computer Vision*. 4956–4965.
 - [79] Zongsheng Yue, Jianyi Wang, and Chen Change Loy. 2023. ResShift: Efficient diffusion model for image super-resolution by residual shifting. *Proceedings of the Advances in Neural Information Processing Systems* (2023).
 - [80] Zongsheng Yue, Qian Zhao, Jianwen Xie, Lei Zhang, Deyu Meng, and Kwan-Yee K Wong. 2022. Blind Image Super-resolution with Elaborate Degradation Modeling on Noise and Kernel. In *IEEE Conference on Computer Vision and Pattern Recognition*. 2128–2138.
 - [81] Roman Zeyde, Michael Elad, and Matan Protter. 2010. On Single Image Scale-up Using Sparse-representations. In *International Conference on Curves and Surfaces*. Springer, 711–730.
 - [82] Kai Zhang, Luc Van Gool, and Radu Timofte. 2020. Deep Unfolding Network for Image Super-resolution. In *IEEE Conference on Computer Vision and Pattern Recognition*. 3217–3226.
 - [83] Kaihao Zhang, Dongxu Li, Wenhan Luo, Wenqi Ren, Björn Stenger, Wei Liu, Hongdong Li, and Ming-Hsuan Yang. 2021. Benchmarking ultra-high-definition image super-resolution. In *Proceedings of the IEEE/CVF international conference on computer vision*. 14769–14778.
 - [84] Kai Zhang, Jingyun Liang, Luc Van Gool, and Radu Timofte. [n. d.]. Designing a Practical Degradation Model for Deep Blind Image Super-resolution. In *Proc. IEEE*.
 - [85] Kai Zhang, Wangmeng Zuo, and Lei Zhang. 2018. Learning a Single Convolutional Super-resolution Network for Multiple Degradations. In *IEEE Conference on Computer Vision and Pattern Recognition*. 3262–3271.
 - [86] Richard Zhang, Phillip Isola, Alexei A Efros, Eli Shechtman, and Oliver Wang. 2018. The Unreasonable Effectiveness of Deep Features as a Perceptual Metric. In *IEEE Conference on Computer Vision and Pattern Recognition*. 586–595.
 - [87] Wenlong Zhang, Yihao Liu, Chao Dong, and Yu Qiao. 2019. Rankrgan: Generative adversarial networks with ranker for image super-resolution. In *Proceedings of the IEEE/CVF International Conference on Computer Vision*. 3096–3105.
 - [88] Xuaner Zhang, Qifeng Chen, Ren Ng, and Vladlen Koltun. 2019. Zoom to learn, learn to zoom. In *Proceedings of the IEEE/CVF Conference on Computer Vision and Pattern Recognition*. 3762–3770.
 - [89] Xindong Zhang, Hui Zeng, Shi Guo, and Lei Zhang. 2022. Efficient Long-range Attention Network for Image Super-resolution. In *European Conference on Computer Vision*. Springer, 649–667.
 - [90] Yulun Zhang, Kunpeng Li, Kai Li, Lichen Wang, Bineng Zhong, and Yun Fu. 2018. Image Super-resolution Using Very Deep Residual Channel Attention Networks. In *European Conference on Computer Vision*. 286–301.
 - [91] Yulun Zhang, Yapeng Tian, Yu Kong, Bineng Zhong, and Yun Fu. 2018. Residual dense network for image super-resolution. In *IEEE Conference on Computer Vision and Pattern Recognition*. 2472–2481.
 - [92] Yulun Zhang, Donglai Wei, Can Qin, Huan Wang, Hanspeter Pfister, and Yun Fu. 2021. Context reasoning attention network for image super-resolution. In *Proceedings of the IEEE/CVF International Conference on Computer Vision*. 4278–4287.
 - [93] Hongyang Zhou, Xiaobin Zhu, Jianqing Zhu, Zheng Han, Shi-Xue Zhang, Jingyan Qin, and Xu-Cheng Yin. 2023. Learning Correction Filter via Degradation-Adaptive Regression for Blind Single Image Super-Resolution. In *Proceedings of the IEEE/CVF International Conference on Computer Vision*. 12365–12375.